Experimental analysis of the response of Fibre Bragg Grating sensors under non-uniform strain field in a twill woven composite

M. Kharshiduzzaman[1], A. Gianneo[1], A. Bernasconi[1,*]

[1] Politecnico di Milano, Dipartimento di Meccanica, Via La Masa 1, 20156 Milano, Italy.

Abstract

Fibre Bragg Grating (FBG) optical sensors are nowadays widely employed for strain measurement for structural health monitoring and in experimental mechanics. Compared to other techniques, i.e. electrical strain gauges, FBG offer immunity to electromagnetic interference and allow for long transmission lead lines. Moreover, thanks to multiplexing interrogation, several sensors can be photo-imprinted into a single fibre core allowing for strain evaluation at multiple locations simultaneously. They have high adaptability to composite materials, particularly because it is possible to be embedded into laminates without affecting their strength and stiffness. FBG strain measurements are based on the detection of the wavelength shift of their peak reflected spectrum. However, subjected to strain gradients, the spectral response of FBG sensors may be distorted and the sharp peak may not be retained. In this work, the response of FBG sensors having different grating

[*] Corresponding author. Tel.: +39-02-2399-8222; fax: +39-02-2399-8263.

E-mail address: andrea.bernasconi@polimi.it.

lengths and bonded to the surface of a carbon fibre reinforced twill woven laminate was analyzed. The analysis combined transfer matrix (T-matrix) with digital image correlation (DIC) methods. DIC technique was used to capture the non-uniform strain fields in the woven composites and measured strains were employed in T-Matrix algorithm to simulate FBG response. Using this approach, the effect of the length of the FBGs grating on the strain measurement is assessed and results discussed. Moreover, it is shown that T-matrix formulation combined with a non-contact strain field measurement technique, as DIC, is an appropriate technique to simulate the behavior of FBGs bonded to composite materials of complex microstructure.

Keywords: Carbon Fiber Reinforced Polymer, Twill Woven, Fiber Bragg Grating (FBG), Digital Image Correlation (DIC), T-matrix.

1. Introduction

Strain-based methods belong to the wide class of structural health monitoring (SHM) techniques that also includes, among others, ultrasonic guided waves [1–3], acoustic emission (AE) [4,5] and dynamic modal data [6,7]. Strain-based methods are very effective, because in general the presence of damage in a structure modifies the local strain distribution under operational loads. Strain based techniques proved to be able to detect the onset of damage, e.g. fatigue cracking, and its subsequent propagation. Both electrical resistance strain gages [8–10] and optical sensors can be successfully used [11–13] to measure local strain fields for monitoring purposes. Due to their intrinsic characteristics, FBG strain monitoring is more suited to structural “hotspots” in large components rather

than wide-area monitoring, as single or a small number of sensors can be used. However, the latter aspect can be overcome thanks to the multiplexing interrogation capability of FBG optical interrogators, where several sensors [14] can be photo-imprinted on a single fibre core (of length up to 10km) thus establishing a quasi-distributed array of sensors for structural monitoring of wide areas [15,16]. The maximum number of gratings than can be interrogated depend on the multiplexing method, ranging from 20 to 1000 on a single fibre [17].

Hence, FBG sensors provide a potential solution for strain based SHM techniques in composites structures as well as adhesively bonded joints. A FBG sensor has several advantages over traditional electrical resistance strain gauges, such as immunity to electromagnetic interference, possibility of long transmission lead lines, applicability in flammable area and serial multiplexing [14,18]. Moreover, due to low weight and small size, FBGs can be embedded in composite laminates with a negligible effect on their mechanical properties [19-22]. FBG strain sensors have been used in order to detect microscopic damages in composite laminates [23], for the investigation of delamination detection in CFRP laminates[24] and for monitoring crack growth in composite joints [25, 26]. For adhesively bonded composite joints, it was shown that an array of FBG sensors can efficiently capture the back face (BF) strain profile, which is a vital parameter for crack detection [27, 28].

Although FBG sensors possess the aforementioned advantages over electrical resistance strain gauges, their response is affected by strain gradient in a different way. In particular, they do not possess the capability of averaging the strain over their gauge length. In facts, when subjected to strain gradients [29] due to structural geometry, cracks, and/or biaxial strain distributions (embedded FBGs) [29, 30], the reflected spectrum does not always

produce the distinctive peaks which are necessary for accurate strain and/or temperature evaluation [31, 32] and peak splitting, reduction of reflectivity and enlargement of the bandwidth occur.

Kang et al.[33] investigated the signal stability and characteristic, in terms of reflectivity and bandwidth, of FBG sensors under different strain gradients and grating lengths with reference to a bending test of an acrylic cantilever beam. They proposed an optimum working range of FBG lengths indicating which particular grating length, as a function of the strain gradient, could be used without peak splitting. However, conclusions hold for an isotropic material under a simplified loading condition (i.e. cantilever beam) and under a simplified (i.e. linear) strain gradient. Therefore at least within the limits of the knowledge of the authors of the present article, the assessment in non-homogeneous materials like in woven fabric composites is still a challenge.

Huang et al. [31] developed Transfer Matrix (T-matrix) formalism to calculate the influence of strain fields on the reflective spectra of Bragg gratings. Peters et al. [32] used this technique for experimental verifications and modified it for high strain gradient applications. The response of FBG sensors for non-homogeneous materials like woven composites has not yet fully investigated using the T-matrix formalism.

In this work, the response of FBG sensors, having three different grating lengths, applied to a twill woven composite under tensile load is analyzed experimentally and discussed with focus on the non-uniform strain field. The relationship between the dimensions of the repeating unit structure of the woven material and the length of the FBG grating is considered, and Digital Image Correlation (DIC) technique is used to capture the heterogeneous strain field.

Nowadays, DIC is a well-established technique to accurately measure the full field surface strain distribution without the need of applying sensors to the surface of the part under examination. Espinosa et al. [34] used DIC strain measurements to investigate damaged composite structures subjected to tensile loading as well as compressive loading [26]. Several authors, like Nicoletto et al [35, 36] and Daggumati et al [29] used DIC technique to capture the full field strain of twill and 5-harness satin weave composites, respectively, under static tension for validation purposes of mesoscale FE analysis. Caminero et al. [37] used DIC method to monitor composite laminates with an open hole configuration, and also studied the performance of adhesively bonded patch repairs under tensile loading conditions. The response of FBG sensors was validated by Schukar et al. [38] using DIC and ESPI (Electronic Speckle Pattern Interferometry).

In this paper, a similar approach based on DIC was adopted for the validation of the reflected spectra of FBGs under heterogeneous strain fields within a woven composite system. A T-matrix algorithm was used to simulate the FBG response using as input the strain field captured by 2D-DIC technique. Finally, experiments were carried out using three different FBGs to compare the results with T-matrix simulations and to draw conclusions about the influence of the length of FBG gratings upon the strain measurements.

2. Experimental

2.1 Experimental Setup

Experiments were performed employing two laminates made of four twill 2x2 woven plies of low modulus carbon fibre (T300) and an epoxy matrix system as described in Fig. 1 (a);

all the plies are oriented at 0° with reference to the longitudinal axis of the specimen. The twill weave configuration created a square pattern of unit cells of $10x10\ mm^2$ as shown in Fig.1 (b).

First, surface of the specimens was prepared for DIC measurements by white painting and creating a speckle pattern by means of a black paint airbrush. Then, static tensile loads were applied to both specimens, Fig. 2(a), up to a maximum force of 8 kN by means of a servo-hydraulic system MTS Landmark™ Testing Solutions, USA, with a capacity of 100 kN. The load was increased in a stepwise manner, with a step of 100 N, to allow for acquisition of images to be processed by DIC.

After the acquisition of these images, the speckled zones were cleaned and FBGs were installed. Draw Tower Gratings (DTG®s) written in Low Bend Loss fiber having three gage lengths of 10 mm, 4 mm and 1 mm, respectively, were bonded on the specimens. The opto-mechanical properties of DTG®s are reported in Table 1 and 2. Particularly, the 10 mm and 4 mm FBGs are single grating strain sensors, whereas the 1 mm ones form an array of four strain gratings arranged consecutively on a single mode fiber. The 10 mm and 4 mm FBGs were surface bonded on specimen #1 and the 1 mm long ones on specimen #2 as reported in Fig. 2 (b)-(c). The installation positions were accurately measured and recorded, to define their respective positions and paths within the characteristic repeating unit of the weave. This was done to allow for comparing the reflected spectra and strains measured by FBGs with the ones obtained by T-matrix simulation based on the strain field captured by DIC. Finally, the tensile tests were repeated, to acquire the spectra reflected by FBGs and measure the strains.

2.2 Strain Field measurement

Digital image correlation (DIC) is an experimental mechanics technique for measuring displacements at the surface of a structure undergoing motion or deformation. Based on measured displacements, surface strains can then be determined (i.e. Green-Lagrangian formulation). For this work, a 2D DIC method was applied for capturing the strain field in the the woven composite strips. A digital single-lens reflex (DSLR) camera (CANON EOS 400D, Tokyo, Japan) with a 100 mm macro lens was used to capture reference (no load applied) and current digital images under tensile load. A tripod was used to fix the camera in such a position that the specimen surface remains parallel to the image sensor. A white light source was used to illuminate the specimen and was not moved during load application and image acquisition of the deformed specimen, to ensure that all images were taken under the same constant lighting conditions.

The regions selected for the random speckle pattern were cleaned with Acetone and marked by applying an adhesive tape at the end of both sides of the specimen. Then, white paint was applied within the portion of the specimens cleaned before, allowed to dry and finally a speckle was created by spraying black paint from an airbrush. The speckle pattern on specimen #1 is illustrated in Figure 3(a). Images were captured with a resolution of 10 (3888x2592) Megapixel and the system was calibrated, obtaining a scale factor value equal to 80 pixels/mm, i.e. 0.0125mm/pixel.

Then, acquired images were post-processed using Ncorr V1.2 [39], an open source 2D digital image correlation program, to obtain the displacement field undergone and subsequently evaluate the 2D strain field. Under the assumption that the gray level intensity of a physical point does not change between the reference image and the deformed one [39], the software creates a mesh of subsets across a Region of Interest (ROI) and finds a

unique point for each subset correlating the images. The step size is the number of pixel the software uses to track subsets, i.e. for a step size of 5 pixels, the software tracks the subset area for every 5 pixels. Ncorr computes the strain field from the Green-Lagrangian strain formulation [39]. However, since these values are typically noisy, Ncorr asks the user to define a strain window. This algorithm, proposed in [40], uses a pointwise least squares estimation, where, assuming a strain window small enough, the displacement field can be approximated as a linear function of the x and y coordinates. Subset size was selected equal to 30 (a 30x30 pixel window) with 15 pixels step size, whereas full field strain measurements were evaluated using a strain window of 15 pixels radius. The latter parameter was chosen as a trade-off between strain accuracy and smoothness. An example of the longitudinal strain field, ε_{yy}, is shown in Figure 3(b) for an 8 kN load level; the strain field reported refers to the red dashed box whose area is equal to $25.4x30\ mm^2$. The strain field is superimposed to the image of the sample in Figure 3(d).

Once the strain field was mapped, strain profiles, see Figure 3(e), were extracted along paths coinciding exactly with lines along which the FBGs that were later installed, as shown in Figure 3(c). It clearly appears that strains along the black dashed line of Figure 3(e) are not constant, with oscillations of 1000 μm/m amplitude for an applied load of 8 kN.

2.3 FBG strain measurement

FBG sensors were conditioned using a Hottinger Baldwin Messtechnik GmbH (HBM) DI410 dynamic optical interrogator. Raw spectra at different load levels were acquired, and then they were post processed off-line according to a peak detection algorithm in order

to calculate strains. More precisely, the implemented algorithm firstly acts as a low-pass filter with filter coefficients equal to the reciprocal of the span (moving average of 100pm), then it finds the two closest bracketing points within 80% of maximum spectrum amplitude, and finally, after differentiation, the peak wavelength is found as the zero-crossing wavelength. This method is illustrated in Figure 4. Once the peak wavelength corresponding to the different load levels was found, strains were determined according to the well-known relationship

$$\frac{\Delta\lambda}{\lambda} = \mathrm{G}\left(1 - \frac{\mathrm{n}^2}{2}\left(\mathrm{p}_{12} + \mathrm{p}_{11}\frac{\varepsilon_{\mathrm{rr}}}{\varepsilon_{\mathrm{zz}}} + \mathrm{p}_{12}\frac{\varepsilon_{\vartheta\theta}}{\varepsilon_{zz}}\right)\right)\varepsilon_{\mathrm{zz}} = (1 - p_e)\varepsilon \qquad (1)$$

where p_{ij} are the photo-elastic coefficient (a typical value of $p_e = 0.22$ was employed for a silica fiber with a germanium doped core), $\Delta\lambda$ the peak wavelength shift from the baseline wavelength (at zero strain) λ and ε_{ij} the strains undergone within the fibre.

2.4 T-Matrix simulation

The numerical model used to simulate the reflected spectra of a FBG sensor subjected to an arbitrary strain profile is based on the transfer matrix approximation (T-matrix) model by Huang et al [41]. This approach, initially proposed by Yamada and Sakuda [42], is a way of solving coupled-mode equations, in a computationally, more efficient way, compared with direct numerical integration. It discretizes a single grating into a series of smaller distinct ones with uniform coupling properties and describes each of them by its own optical transfer matrix F_i. Then, by combining all the F_i matrices, the reflectivity spectrum of FBG sensor can be obtained for a given strain profile. Therefore, once the

strain profile is known by experimental/numerical methods, the reflected spectrum of FBG sensor for that strain profile can be estimated by the T-matrix model.

The FBG is defined as a small periodical perturbation of the effective reflective index δn_{eff} of the photosensitive optical fiber core and it can be described as [41]

$$\delta n_{eff}(x) = \overline{\delta n_{eff}} \left\{1 + \upsilon cos\left[\frac{2\pi}{\Lambda_0} x + \varphi(x)\right]\right\} \quad (2)$$

where, $\overline{\delta n_{eff}}$ is the "dc" index change spatially averaged over a grating period, υ the fringe visibility, Λ_0 the nominal grating period, $\varphi(x)$ the grating chirp and x the axial direction along the fibre length. The T-matrix for the n-th section can be obtained as [39]

$$T_n = \begin{pmatrix} \cosh(\gamma_B \Delta x) - i\frac{\hat{\sigma}}{\gamma_B} sinh(\gamma_B \Delta x) & -i\frac{k}{\gamma_B} sinh(\gamma_B \Delta x) \\ -i\frac{k}{\gamma_B} sinh(\gamma_B \Delta x) & \cosh(\gamma_B \Delta x) + i\frac{\hat{\sigma}}{\gamma_B} sinh(\gamma_B \Delta x) \end{pmatrix} \quad (3)$$

where Δx is the length of each segment, $\hat{\sigma} = 2\pi n_{eff}\left(\frac{1}{\lambda} - \frac{1}{\lambda_D}\right) + \frac{2\pi}{\lambda}\overline{\delta n_{eff}} - \frac{1}{2}\phi'(x)$ is the general "dc" self-coupling coefficient where $\phi'(x) = \frac{d\phi}{dx}$ and $\lambda_D = 2\pi n_{eff}\Lambda_0$ is the design wavelength. $\gamma_B = \sqrt{k^2 - \hat{\sigma}^2}$ where $k = \frac{\pi}{\lambda}\upsilon\overline{\delta n_{eff}}$ is the "ac" coupling coefficient.

Finally, the transfer matrix for the whole FBG sensor can be computed by the product of all the n-th T-matrices and the reflection spectrum R can be found with the following expression [39]

$$T = \prod T_n \begin{pmatrix} T_{11} & T_{12} \\ T_{21} & T_{22} \end{pmatrix}, R = \left(\frac{T_{21}}{T_{11}}\right)^2 \quad (4)$$

As already pointed out, the grating is divided into N smaller sections having uniform coupling properties. However the number of sections N cannot be arbitrarily large, and it is constrained by the inequality $N \ll \frac{2n_{eff}L}{\lambda}$ since several grating periods are required within a section for complete coupling [42]. The input of T-matrix model is the strain profile $\varepsilon(x)$, in this work measured by DIC, along the length of the grating of each FBG sensor (x indicates the local coordinate axis parallel to the sensor, with origin in one of its ends, whereas strains were extracted along the Y axis of the global reference system shown in Figure 3). The grating period can be obtained from a modified effective one [43].

$$\tilde{\Lambda}(x) = [1 + (1 - p_e)\varepsilon(x) + (1 - p_e)x\varepsilon'(x)] \quad (5)$$

The aforementioned model was implemented in a Matlab R2016b script to obtain the reflectivity spectrum of the Bragg grating used in this work. More precisely, the implemented algorithm iterates through the wavelengths with a resolution of 1 pm. The opto-mechanical characteristics of the FBG used for response-T-matrix are shown in Table 2. In this work, the number of sections over the grating length was chosen equal to 100. A value of 100 is sufficient for accurate modelling [43] and we verified that increasing the value of N beyond 100 does not significantly increase the accuracy, whereas computational times are increased significantly.

3. Results and discussion

In this section, we present, discuss and compare the spectra and the strain values, obtained:

- directly by processing the experimental spectrum recorded by the FBG interrogator, using the peak detection algorithm (indicated by "FBG measured" in the following text)
- by processing with T-matrix the strain values obtained by DIC measurements, extracted along the paths coinciding with the position of the FBG gratings (indicated by "T-matrix simulated" in the following text).

The reflected spectra and the corresponding strain values were obtained for all load levels for the 10 mm, 4 mm and 1 mm FBGs. Then, FBG measured and T-matrix simulated strains were compared with the average strain determined from DIC strain maps using a virtual extensometer whose gauge length was equal to 10 mm, i.e. at least as great as the characteristic repeating unit of the weave as suggested within the ASTM D3039 standard [44]. Finally, the response of the FBG sensor was simulated by exploring a rectangular portion of the strain field recorded by DIC. A virtual FBG sensor was positioned on a grid of 13 mm x 13 mm, large enough to enclose one representative volume of the woven material, and displaced with a step of 1 mm. Then, the strain values along the FBG length were extracted from DIC data and processed by T-matrix to evaluate the strain value measure by the virtual FBG at every position.

3.1 FBG measured and T-matrix simulated results for the 10 mm FBG sensor

For the 10 mm long FBGs, Figure 5 shows the superimposed FBG measured (black lines) and the T-matrix simulated (blue lines) reflected spectra compared with the FBG measured reflected spectra when no strain is applied (red lines), which is labelled as 0kN in the figures. The comparison between FBG measured and T matrix simulated spectra indicates a fairly good agreement. Both the FBG measured and the T-matrix simulated response of a 10 mm FBG sensor do not provide a single distinctive peak, as chirping and peak splitting occur even at small loads and, hence, low strain values. As the input strain along a 10 mm FBG length is highly non-uniform (Fig. 4 shows the typical band-like variation of strains on the surface of the specimen), T-matrix analysis confirms that peak splitting is related to this non-uniform strain profile along the length of the FBG.

T-matrix results agree well with FBG results also in terms of strain values. Comparison of FBG measured strain values with the T matrix simulated strain values is reported in Figure 6, where also the DIC strain (virtual extensometer) values are reported. It is observed that, at low load level, i.e. smaller strain gradient, FBG strain readings are comparable to the DIC averaged values. However, both considerably differ from DIC ones.

As already pointed out, due to the presence of a strain gradient, chirping of grating occurred, leading to peak splitting. This was observed in both FBG and T-matrix results. Due to this chirping effect, no unique distinctive peak was produced by the reflected FBG spectrum even at small load levels, and consequently strain evaluations were affected. The peak of the reflected spectrum from FBG sensor is a fundamental feature for strain

measurement and therefore, when there is no distinctive peak, the strain measurement may become inaccurate and induce the peak detection algorithms to errors.

Moreover, the response depends on the position of the grating. The response of a virtual 10 mm FBG sensor was simulated by T-matrix simulation for varying positions of the sensors, exploring a rectangular 13 mm x 13 mm portion of the strain field recorded by DIC. Values of the longitudinal strain obtained by T-matrix simulation are reported in Figure 7 as a function of the location of the centre of the virtual FBG sensor. It appears that the measured strain values are not uniform across the explored area, thus confirming the inability of the 10 mm long sensor to average strain. As reported in ASTM D3039 [44]:"*when testing woven fabric laminates, gage selection should consider the use of an active gage length that is at least as great as the characteristic repeating unit of the weave*". However, contrary to electrical resistance strain gauges, where one would typically employ a measuring grid large enough to average inhomogeneous strain fields, in this case, large grating lengths are counterproductive.

3.2 FBG measured and T-matrix simulated results for the 4 mm FBG sensor

Figure 8 shows the reflected spectra of the 4 mm FBG sensor superimposed to the T-matrix simulated ones, the latter based on the non-uniform strain profile extracted along the same segment from the DIC measured field. Also plotted is the FBG measured reflected spectra when no strain is applied. We can observe that the experimental spectral response of the 4 mm FBG retains the main characteristic needed for a correct strain estimation, i.e. a single peak, up to 7 kN. Small chirping effect is present, but not as dominant as in the case of the

10 mm FBG, where the peak was split at low loads. Therefore, these observations confirmed that, reducing the gauge length over a non-uniform strain path, peak splitting can be avoided.

This is particularly true for experimental data, where a unique peak is preserved up to 7kN, even though the spectrum shape is losing sharpness and peak splitting starts to appear at the left and right sides of the spectrum. The latter behavior is particularly true for load levels above 5kN. Anyway, for the 4 mm FBG, peak splitting is not as dominant as for 10mm FBG and the detection of a unique peak is still possible. Conversely, the T-matrix simulated spectra display earlier signs of chirping at lower loads, with peak splitting appearing at 4 kN.

The comparison between FBG measured, T-matrix simulated and DIC strains (virtual extensometer) is reported in Figure 9. FBG measured strain values agree well with DIC strain values all over the investigated load range (0-8kN). Regarding T-matrix simulated ones, with the exception of the 4 kN and the 8kN load levels, a fairly good agreement can be found: results are randomly positioned around the "true" experimental values. It appears that even if peak splitting occurred at 4kN, it did not always affect the T-matrix simulated strain values.

In this case, the shorter FBG, less than one-half of the 10mm grating length, did not experience considerable chirping as the 10 mm FBG. However, these results do not indicate that a 4mm FBG is suitable for strain measurement over a $10x10mm^2$ unit cell. In fact, it must be pointed out that results were obtained by placing the grid in one specific position. To check this, the same analysis of the response of a 4 mm virtual FBG sensor over a 13 mm x 13 mm area as the one previously performed with a 10 mm FBG was conducted. The

results reported in Figure 10 show that with 4 mm FBG sensors strains are not averaged and differences of the order of 1000 μm/m appear. Conversely, local strains are captured better, although the strain pattern is distorted with respect to the DIC one. Therefore, the 4 mm FBG appears to be neither suitable for local measurements, nor capable of measuring an average value.

3.3 FBG measured and T-matrix simulated results for the 1 mm FBG sensors

Finally, the reflected spectrum of the four 1 mm FBG was measured experimentally and simulated by the T-matrix method. The reflected spectra were simulated for the 4 different positions within the repeating unit cell according to an array of 4 FBGs having 1 mm gage length as the one experimentally employed.

Figure 11 shows the spectral responses, FBG measured and the T-matrix simulated. Comparing the FBG measured and the T-matrix simulated raw spectra, it can be pointed out an excellent agreement for all the four considered positions along the repeating unit of the twill structure. It can be seen that, for all the positions, the reflected spectra of the 1 mm FBGs produce a distinctive peak and peak splitting phenomenon is absent up to 8 kN. This makes this gage length suitable for capturing local stresses in presence of high strain gradients as in twill woven composite studied herein. However, this feature denotes that values are read over small regions, resulting in local strain values that may differ from average ones, i.e. those evaluated by averaging the values measured by DIC.

In facts, as shown in Figure 12 (a)-(d), depending on their position within the twill weave repeating unit structure, strain values sensed by the FBGs considerably differ from each

other and in some cases from the DIC values (virtual extensometer). A 1 mm long FBG seems to capture weel local strains at small scale length. This is clearly shown in Figure 13 by the results of the simulation of the response of a 1 mm FBG sensor displaced with a step of 1 mm over a 13 mm x 13 mm area of the strain field recorded by DIC. It appears clearly that the strains recorded by these FBGs are localized strains and the strain pattern is very similar to the one captured by DIC. Therefore, it is concluded that, although not prone to chirping, the 1 mm FBG provides strain values close to average ones only at specific locations. However, as the length of the sensor is comparable to the uncertainty of the position of the gratings along the fibre, this type of sensor is at risk of measuring values that are much larger or lower than the average strain.

In theory, to compensate for this effect while capturing strain profiles, an array containing a large number of 1mm grating length FBG sensors could be implemented by placing them along the repeating cell and subsequently averaging measured strains. Average strain values of the four 1 mm FBGs are presented in Figure 14. In this case, excellent agreement between averaged strains measured by the array of four 1mm FBGs and averaged DIC measured ones is found. However, in practice it is very difficult to control the exact position of such short sensors and one may face the risk of placing all sensors at locations resulting in the least accurate measurements. Moreover, the price of an array of four or more sensors may exceed that of solutions already existing for the surface application of FBG sensors to areas with non-uniform strains, like woven composites, that are commercial available in the form of FBG sensors applied to flexible patches to be bonded or (in the case of metallic substrates) welded to the area of measurement.

In order to understand if single sensor based solutions other than arrays or flexible patches are possible for the material used in this work or, in general, for other woven composite patterns, the method based on DIC and T-matrix applied herein was applied to investigate the effect of the length of the grating, to explore other FBG lengths than 1 mm, 4 mm and 10 mm. In fact, the method proved to allow for simulating the reflected spectra of the sensors studied in this work, with good agreement with the response of real FBGs. Therefore, the T-matrix simulation was applied to other virtual sensors, aiming at identifying by simulation a possible more suitable grating length, at least for the material studied herein. The response of FBGs of 6 mm and 12 mm length was simulated over the 13 mm x 13 mm area previously selected for the simulation of the response of the 1,4 and 10 mm FBGs and results are presented in Figure 15. It appears clearly that both sensors are unable to capture an average strain, as results fluctuate like in the previous cases.

4. Conclusions and further developments

The spectral response of FBG sensors having different gauge lengths, ranging from 1 to 10 mm applied to a twill 2x2 woven CFRP composite were studied in this work.

Based on the results presented in this paper, the following conclusions can be drawn:

- FBGs having smaller gage length, i.e. 1 millimeters, produce sharp peaks of reflected spectra even when non-uniform strain fields occur within the unit cell, allowing for accurately measuring local strains; however, strains measured by 1 mm FBG sensor are basically localized values and therefore differ from average ones;

- result of the strain measurements with the 4mm FBG are in good agreement with average ones; however, peak splitting occurred at higher loads only and the analysis of the effect of the position of the grating within the repeating unit structure allowed to conclude that they are not suitable for local measurements nor for averaging strains along their length;
- results of the strain measurement with the 10mm FBG are in poorer agreement with average ones and chirping appears even for low applied loads; even if the FBG length is larger than the dimension of the unit cell of the woven material, measurements appear as less accurate
- simulation of the behavior of all the FBGs by the T-matrix formalism based on DIC measured strains yielded results in good agreement with experimental data; therefore, the T-matrix formulation appears as a powerful technique to simulate and predict the behavior of FBGs of different length in an inhomogeneous strain field determined by the weave repeating unit structure of a woven composite;
- a preliminary study was conducted using DIC combined with the T matrix method to identify a possible more appropriate length and position of the sensors within the repeating unit structure of the woven composite; the effect of the position within the unit cell of the woven material was investigated by extracting strain values from the map of values collected by DIC along different lines and processing them by T-matrix . These virtual experiments did not allow for determining an optimal grating length allowing for capturing an average strain, at least in the range of 1 mm to 12 mm FBG lengths. Therefore, at the moment the most suitable alternative to averaging strain values recorded by numerous 1 mm FBGs appears to be to the use of FBGs immersed into flexible patches that can homogenize the strains sensed by

the sensor. Nevertheless, results confirm the usefulness of the method, that could be used to predict the response of FBGs before applying them to other composites with a different microstructure.

5. Acknowledgements

Consorzio Spinner, Bologna, Italy, funded the work of Md Kharshiduzzaman within the framework of "Sovvenzione Globale Spinner 2013", for the project "Sviluppo, caratterizzazione e modellazione di strutture in materiale composito "intelligente" (prot. n. 067-dott).

References

[1] Su Z, Ye L. Identification of Damage Using Lamb Waves: From Fundamentals to Applications. Springer Science & Business Media; 2009.

[2] Giurgiutiu V. 6 – GUIDED WAVES. Struct. Heal. Monit., 2008, p. 185–238. doi:10.1016/B978-012088760-6.50007-6.

[3] Rose JL. Ultrasonic Guided Waves in Solid Media. Cambridge University Press; 2014.

[4] Gutkin R, Green CJ, Vangrattanachai S, Pinho ST, Robinson P, Curtis PT. On acoustic emission for failure investigation in CFRP: Pattern recognition and peak frequency analyses. Mech Syst Signal Process 2011;25:1393–407. doi:10.1016/j.ymssp.2010.11.014.

[5] Grosse CU. Introduction. Acoust. Emiss. Test., Berlin, Heidelberg: Springer Berlin Heidelberg; n.d., p. 3–10. doi:10.1007/978-3-540-69972-9_1.

[6] Rolek P, Bruni S, Carboni M. Condition monitoring of railway axles based on low frequency vibrations. Int J Fatigue 2016;86:88–97. doi:10.1016/j.ijfatigue.2015.07.004.

[7] Giurgiutiu V. High-Frequency Vibration SHM with PWAS Modal Sensors – the Electromechanical Impedance Method. Struct. Heal. Monit. with Piezoelectric Wafer Act. Sensors, 2014, p. 509–72. doi:10.1016/B978-0-12-418691-0.00011-3.

[8] Zhang Z, Shang JK, Lawrence F V. A Backface Strain Technique for Detecting Fatigue Crack Initiation in Adhesive Joints. J Adhes 1995;49:23–36. doi:10.1080/00218469508009975.

[9] Crocombe AD, Ong CY, Chan CM, Wahab MMA, Ashcroft IA. Investigating Fatigue Damage Evolution In Adhesively Bonded Structures Using Backface Strain Measurement. J Adhes 2002;78:745–76. doi:10.1080/00218460213835.

[10] Shenoy V, Ashcroft IA, Critchlow GW, Crocombe AD, Abdel Wahab MM. An investigation into the crack initiation and propagation behaviour of bonded single-lap joints using backface strain. Int J Adhes Adhes 2009;29:361–71. doi:10.1016/j.ijadhadh.2008.07.008.

[11] Bernasconi A, Carboni M, Comolli L. Monitoring of fatigue crack growth in composite adhesively bonded joints using Fiber Bragg Gratings. Procedia Eng 2011;10:207–12. doi:10.1016/j.proeng.2011.04.037.

[12] Canal LP, Sarfaraz R, Violakis G, Botsis J, Michaud V, Limberger HG. Monitoring strain gradients in adhesive composite joints by embedded fiber Bragg grating sensors. Compos Struct 2014;112:241–7. doi:10.1016/j.compstruct.2014.02.014.

[13] Bernasconi A, Carboni M, Comolli L, Galeazzi R, Gianneo A, Kharshiduzzaman M. Fatigue Crack Growth Monitoring in Composite Bonded Lap Joints by a Distributed

Fibre Optic Sensing System and Comparison with Ultrasonic Testing. J Adhes 2016;92:739–57. doi:10.1080/00218464.2015.1123153.

[14] Othonos A, Kalli K, Pureur D, Mugnier A. Fibre Bragg Gratings. Wavel. Filters Fibre Opt., Springer Berlin Heidelberg; 2006, p. 189–269. doi:10.1007/3-540-31770-8_6.

[15] Schizas C, Stutz S, Botsis J, Coric D. Monitoring of non-homogeneous strains in composites with embedded wavelength multiplexed fiber Bragg gratings: A methodological study. Compos Struct 2012;94:987–94. doi:10.1016/j.compstruct.2011.09.014.

[16] Kinet D, Mégret P, Goossen K, Qiu L, Heider D, Caucheteur C. Fiber Bragg Grating Sensors toward Structural Health Monitoring in Composite Materials: Challenges and Solutions. Sensors 2014;14:7394–419. doi:10.3390/s140407394.

[17] Minneman MP et al. Very High Sensor-Density Multiplexing using a Wavelength-to-Time Domain Reflectometry Approach based on a Rapidly Swept Akinetic-Laser. Proc. SPIE 9634, 24th International Conference on Optical Fibre Sensors, 96342B (28 September 2015); doi: 10.1117/12.2205455

[18] Sharpe WN. Springer Handbook of Experimental Solid Mechanics. Boston, MA: Springer US; 2008. doi:10.1007/978-0-387-30877-7.

[19] Herszberg I, Li HCH, Dharmawan F, Mouritz AP, Nguyen M, Bayandor J. Damage assessment and monitoring of composite ship joints. Compos Struct 2005;67:205–16. doi:10.1016/j.compstruct.2004.09.017.

[20] Li HCH, Herszberg I, Davis CE, Mouritz AP, Galea SC. Health monitoring of marine composite structural joints using fibre optic sensors. Compos Struct 2006;75:321–7. doi:10.1016/j.compstruct.2006.04.054.

[21] Silva-Muñoz RA, Lopez-Anido RA. Structural health monitoring of marine composite structural joints using embedded fiber Bragg grating strain sensors. Compos Struct 2009;89:224–34. doi:10.1016/j.compstruct.2008.07.027.

[22] Papantoniou A, Rigas G, Alexopoulos ND. Assessment of the strain monitoring reliability of fiber Bragg grating sensor (FBGs) in advanced composite structures. Compos Struct 2011;93:2163–72. doi:10.1016/j.compstruct.2011.03.001.

[23] Okabe Y, Mizutani T, Yashiro S, Takeda N. Detection of microscopic damages in composite laminates. Compos Sci Technol 2002;62:951–8. doi:10.1016/S0266-3538(02)00009-X.

[24] Takeda S, Okabe Y, Takeda N. Delamination detection in CFRP laminates with embedded small-diameter fiber Bragg grating sensors. Compos Part A Appl Sci Manuf 2002;33:971–80. doi:10.1016/S1359-835X(02)00036-2.

[25] Jones R, Galea S. Health monitoring of composite repairs and joints using optical fibres. Compos Struct 2002;58:397–403. doi:10.1016/S0263-8223(02)00235-0.

[26] Palaniappan J, Ogin SL, Thorne AM, Reed GT, Crocombe AD, Capell TF, et al. Disbond growth detection in composite-composite single-lap joints using chirped FBG sensors. Compos Sci Technol 2008;68:2410–7. doi:10.1016/j.compscitech.2007.09.020.

[27] Bernasconi A, Kharshiduzzaman M, Anodio LF, Bordegoni M, Re GM, Braghin F, et al. Development of a Monitoring System for Crack Growth in Bonded Single-Lap Joints Based on the Strain Field and Visualization by Augmented Reality. J Adhes 2014;90:496–510. doi:10.1080/00218464.2013.857606.

[28] Bernasconi A, Comolli L. An investigation of the crack propagation in a carbon fiber bonded joint using backface strain measurements with FBG sensors. In: Liao Y, Jin W, Sampson DD, Yamauchi R, Chung Y, Nakamura K, et al., editors. OFS2012 22nd Int.

Conf. Opt. Fiber Sens., International Society for Optics and Photonics; 2012, p. 84214Y–84214Y–4. doi:10.1117/12.975143.

[29] Daggumati S, Baere I De, Paepegem W Van, Degrieck J, Xu J, Lomov S V, et al. Local Damage in a 5 – Harness Satin Weave Composite Under Static Tension : Part I - Experimental Analysis. Compos Sci Technol 2011;71:1–24. doi:10.1016/j.compscitech.2010.07.002.

[30] Lai M, Karalekas D, Botsis J. On the effects of the lateral strains on the fiber bragg grating response. Sensors (Switzerland) 2013;13:2631–44. doi:10.3390/s130202631.

[31] Huang S, Ohn MM, Measures RM. Phase-based Bragg intragrating distributed strain sensor. Appl Opt 1996;35:1135–42. doi:10.1364/AO.35.001135.

[32] Peters K, Studer M, Botsis J, Iocco A, Limberger H, Salathé R. Embedded optical fiber Bragg grating sensor in a nonuniform strain field: Measurements and simulations. Exp Mech 2001;41:19–28. doi:10.1007/BF02323100.

[33] Kang DH, Park SO, Hong CS, Kim CG. The signal characteristics of reflected spectra of fiber Bragg grating sensors with strain gradients and grating lengths. NDT E Int 2005;38:712–8. doi:10.1016/j.ndteint.2005.04.006.

[34] Espinosa HD, Hild F, Laurin F, Charrier J-S, Lévêque D, Maire J-F, et al. Full-field measurements and identification in Solid Mechanics Determination of the properties of composite materials thanks to digital image correlation measurements. Procedia IUTAM 2012;4:106–15. doi:10.1016/j.piutam.2012.05.012.

[35] Nicoletto G, Anzelotti G, Riva E. Mesoscopic strain fields in woven composites: Experiments vs. finite element modeling. Opt Lasers Eng 2009;47:352–9. doi:10.1016/j.optlaseng.2008.07.009.

[36] Anzelotti G, Nicoletto G, Riva E. Mesomechanic strain analysis of twill-weave composite lamina under unidirectional in-plane tension. Compos Part A Appl Sci Manuf 2008;39:1294–301. doi:10.1016/j.compositesa.2008.01.006.

[37] Caminero MA, Lopez-Pedrosa M, Pinna C, Soutis C. Damage monitoring and analysis of composite laminates with an open hole and adhesively bonded repairs using digital image correlation. Compos Part B 2013;53:76–91. doi:10.1016/j.compositesb.2013.04.050.

[38] Schukar VG, Kadoke D, Kusche N, Muenzenberger S, Gruender K-P, Habel WR. Validation and qualification of surface-applied fibre optic strain sensors using application-independent optical techniques. Meas. Sci. Technol. 2012;23: 085601-09 doi:10.1088/0957-0233/23/8/085601

[39] Blaber J, Adair B, Antoniou A. Ncorr: Open-Source 2D Digital Image Correlation Matlab Software. Exp Mech 2015;55:1105–22. doi:10.1007/s11340-015-0009-1.

[40] Pan B, Asundi A, Xie H, Gao J. Digital image correlation using iterative least squares and pointwise least squares for displacement field and strain field measurements. Opt Lasers Eng 2009;47:865–74. doi:10.1016/j.optlaseng.2008.10.014.

[41] Huang S, LeBlanc M, Ohn MM, Measures RM. Bragg intragrating structural sensing. Appl Opt 1995;34:5003–9. doi:10.1364/AO.34.005003.

[42] Yamada M, Sakuda K. Analysis of almost-periodic distributed feedback slab waveguides via a fundamental matrix approach. Applied Optics 1987; 26: 3474-78. doi:10.1364/AO.26.003474

[43] Prabhugoud M, Peters K. Modified Transfer Matrix Formulation for Bragg Grating Strain Sensors. J Light Technol 2004;22:2302–9. doi:10.1109/JLT.2004.833281.

[44] ASTM International. Astm D3039/D3039M. Annu B ASTM Stand 2014:1–13. doi:10.1520/D3039.

Table. 1: Main Properties of employed Draw Tower Fiber Bragg Gratings (DTG®s)

FBG length	Number of Gratings	Nominal Wavelength [nm]	Actual Wavelength [nm]	Reflectivity [%]
1mm	4	[1530;1540;1550;1560]	[1530.02;1539.85;1549.79;1559.72]	[0.3;0.3;0.3;0.3]]
4mm	1	1550	1549.91	10.4
10mm	1	1550	1549.93	40.6

Table 2: Characteristics of FBG optical sensor used for simulation.

Simbol	**Value**	**Description**
n_{eff}	1.46	Refractive index of the fibre
ν	1	Fringe visibility
p_e	0.22	Photoelastic cofficient
λ_B	1550 (nm)	Bragg wavelength
$\overline{\delta n_{eff}}$	5.510^{-5}	Variation of refractive index
N	100	Number of sections of the grating length
L	Variable (mm)	Length of the Bragg grating

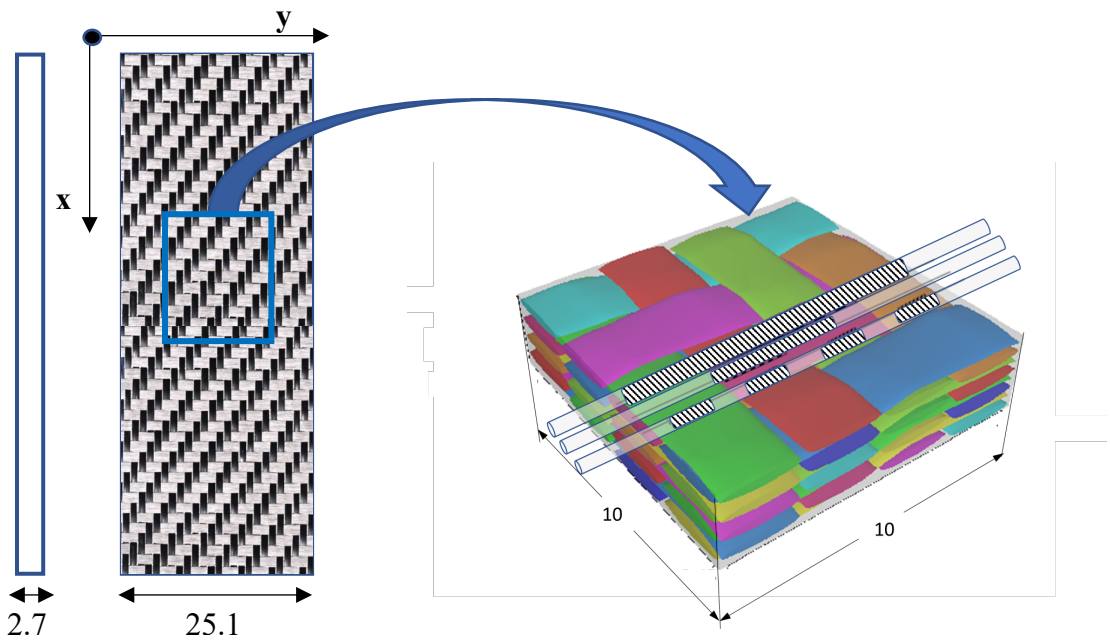

Figure 1: (a) 4 ply twill woven composite specimen, (b) detail of twill woven characteristic repeating unit structure with surface bonded 10, 4, 1 mm FBG locations (all dimensions are in mm)

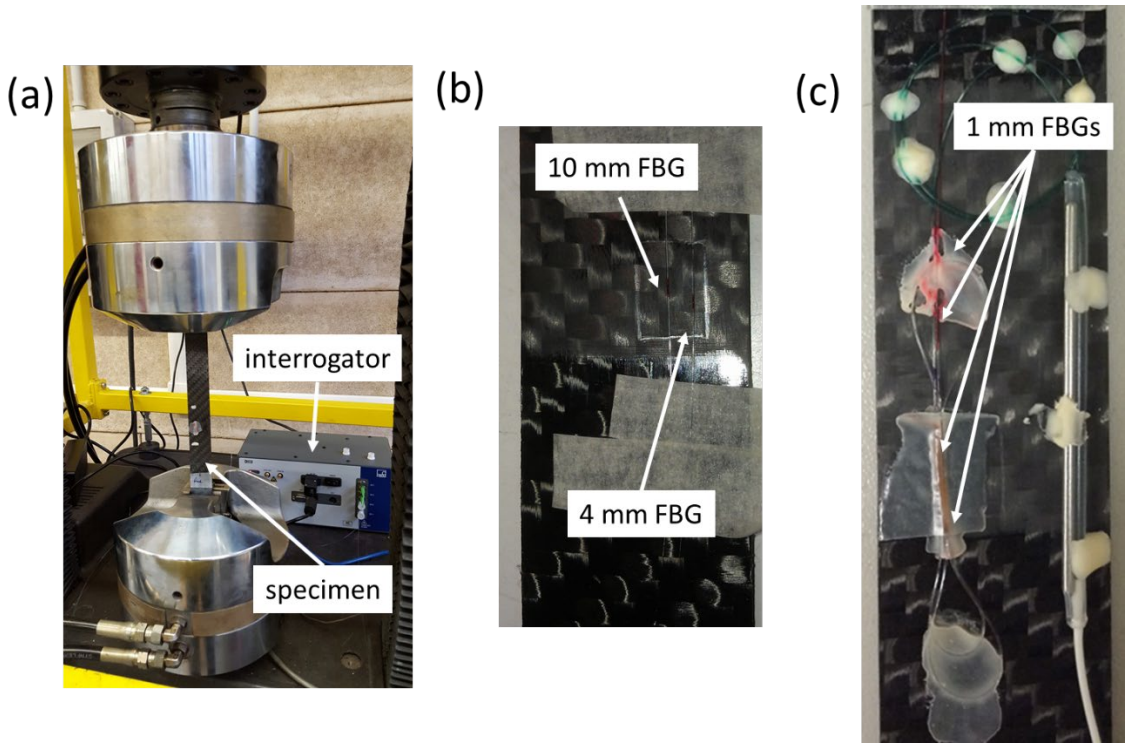

Figure 2: Experimental setup: (a) specimen #2 under tensile load and HBM DI410 optical interrogator (b) specimen #1 with two FBG sensors of 10mm and 4mm grating length respectively (c) specimen #2 with an array of four 1mm FBGs.

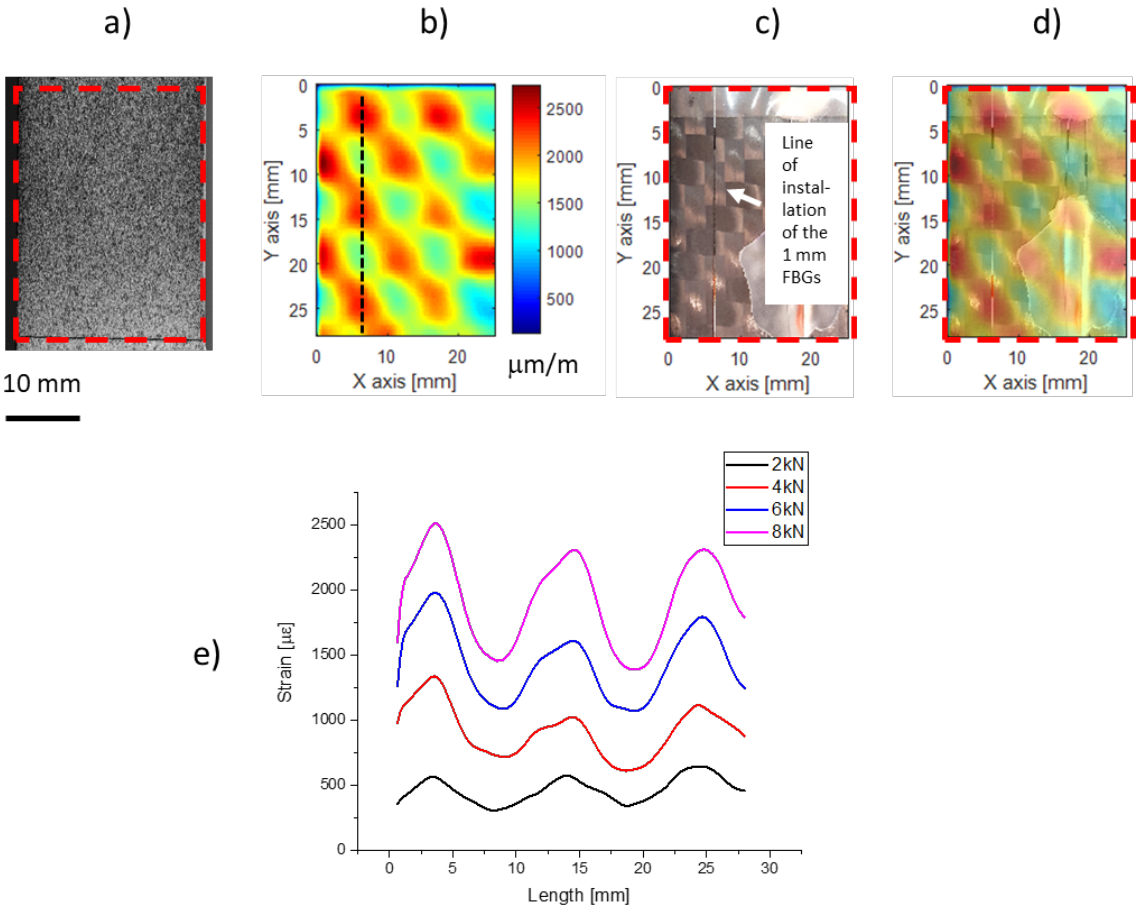

Figure 3: Digital Image Correlation: (a) speckle pattern on specimen #1, (b) longitudinal DIC strain field map at 8kN, (c) image of the specimen under test with an array of four 1 mm FBGs, (d) strain field with superimposed image of the specimen under test, (e) longitudinal strain profile at different load levels along the black dotted extraction path.

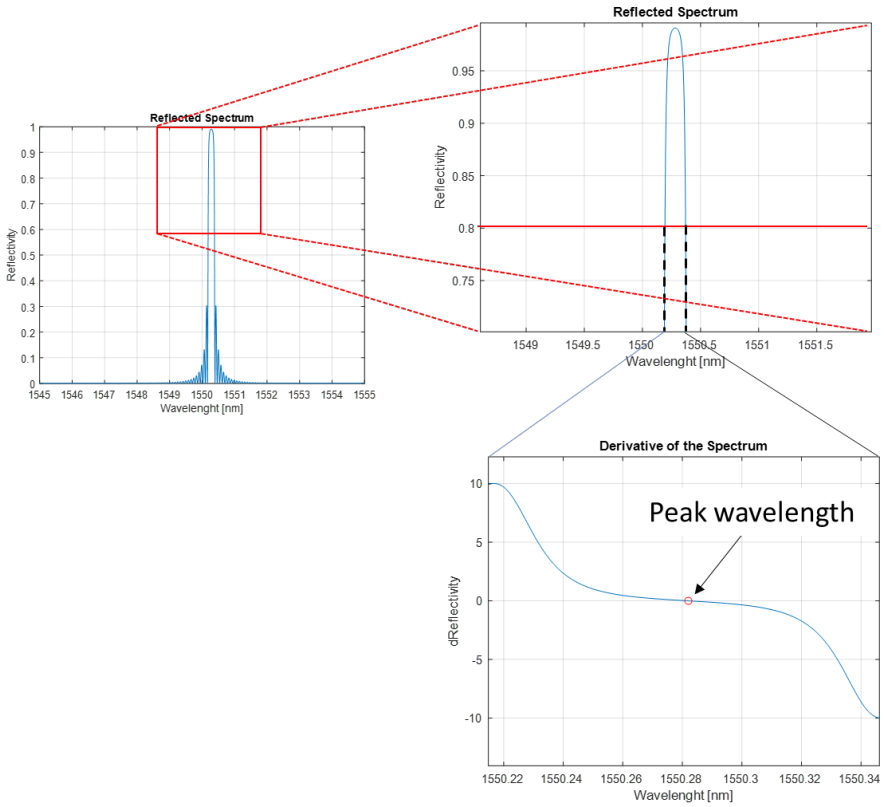

Figure 4: Illustration of the peak detection algorithm

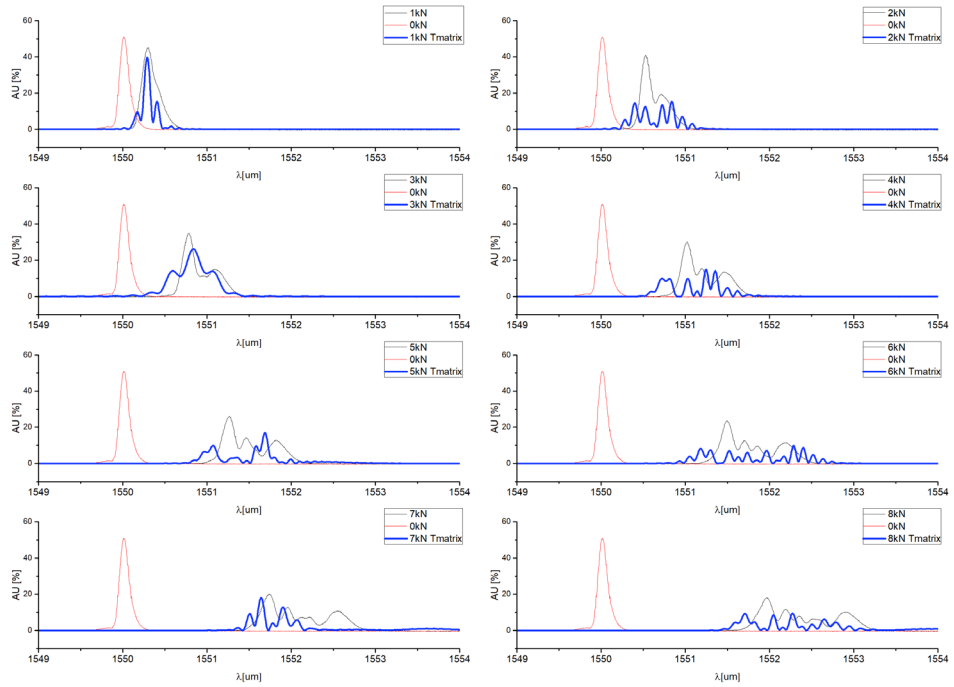

Figure 5: 10mm FBGs measured raw spectra and T-matrix simulated spectra for increasing applied load, superimposed to the baseline with no strain applied (0 kN load).

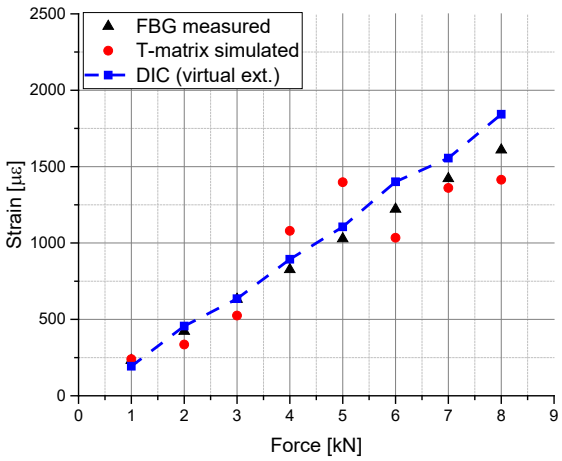

Figure 6: Comparison between experimental, simulated and averaged DIC measured strain for 10mm FBG

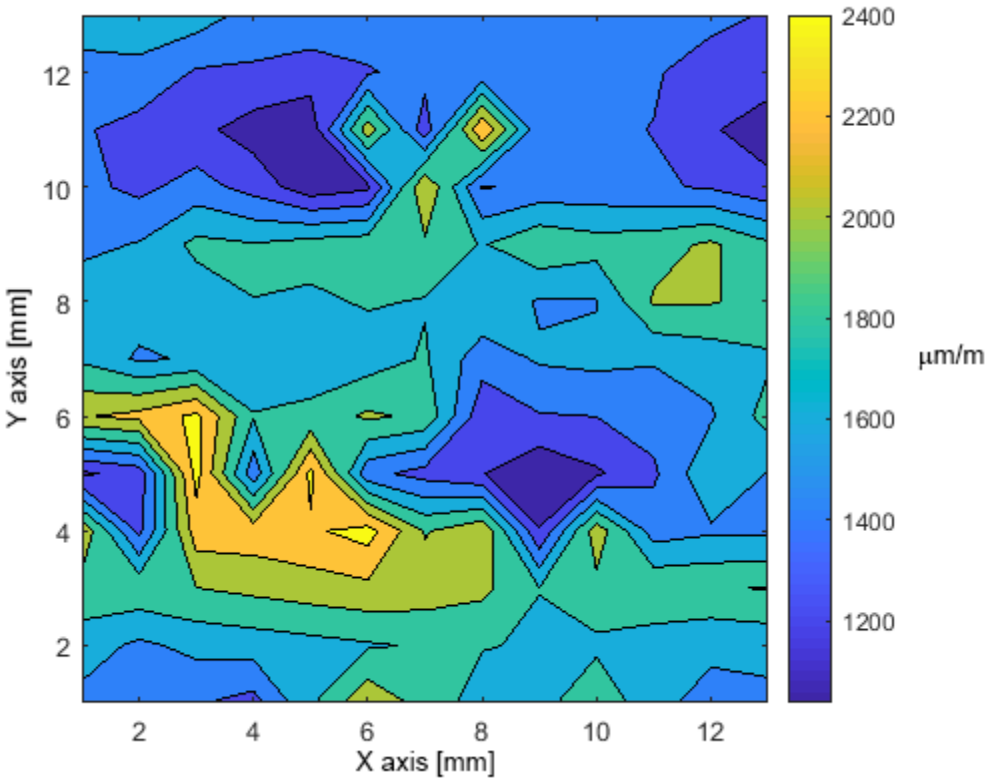

Figure 7: T-matrix simulated response of FBGs of 10 mm length over a 13 mm x 13 mm area of the DIC strain field

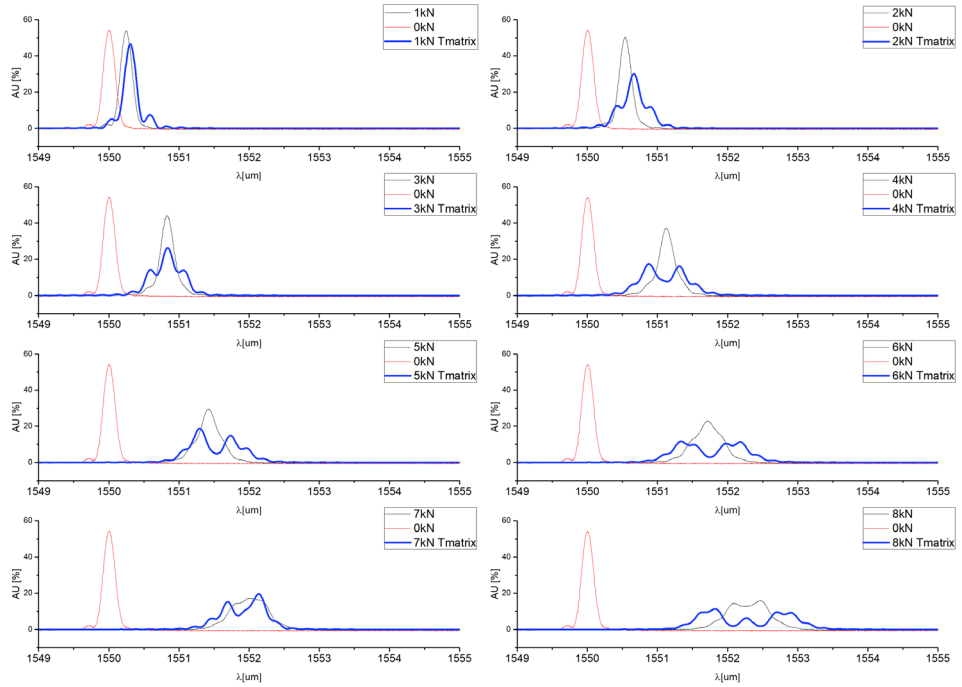

Figure 8: 4mm FBG experimental raw spectra and T-matrix simulated spectra for increasing applied load, superimposed to the baseline with no strain applied (0 kN load).

.

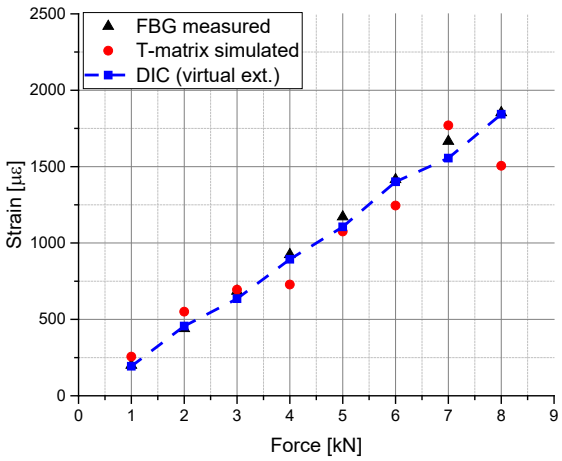

Fig. 9: Comparison between experimental, simulated and averaged DIC measured strain for 4mm FBGs.

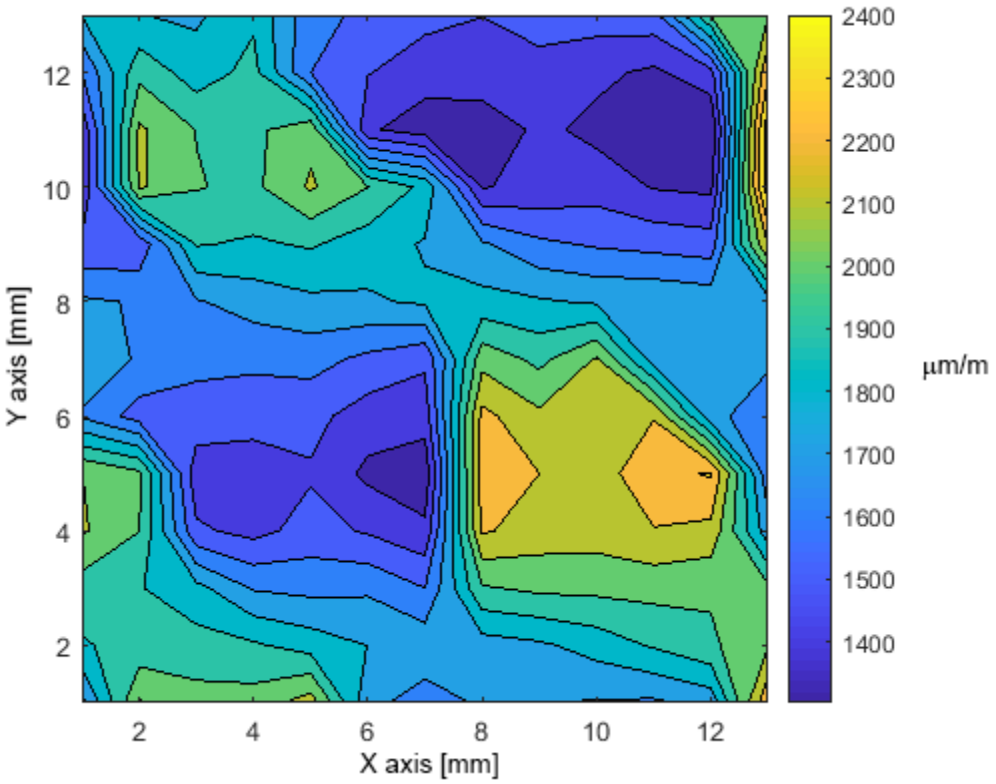

Figure 10: T-matrix simulated response of FBGs of 4 mm length over a 13 mm x 13 mm area of the DIC strain field

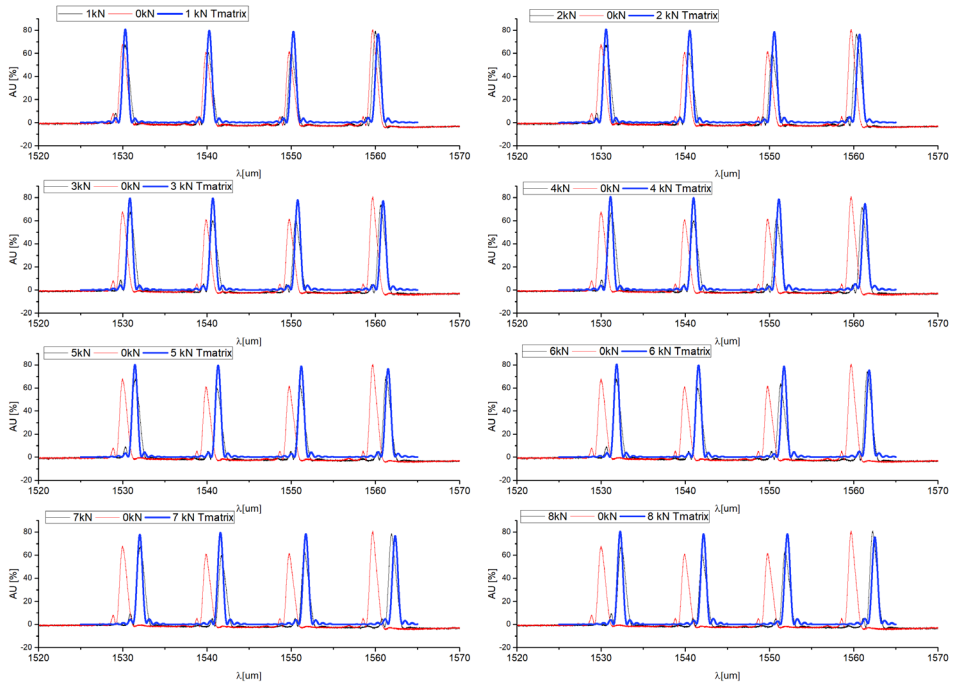

Figure 11: 1mm FBGs experimental raw spectra and T-matrix simulated spectra for increasing applied load, superimposed to the baseline with no strain applied (0 kN load).

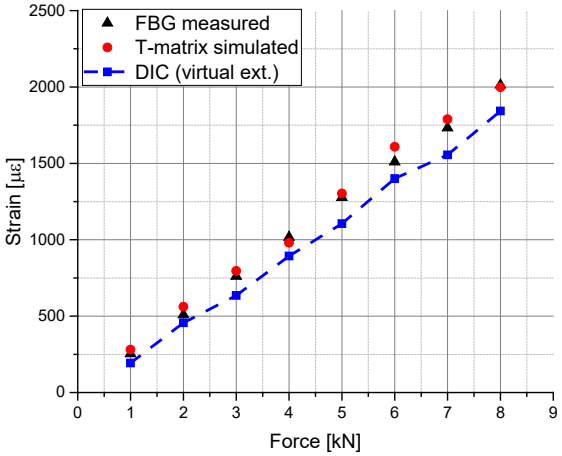

(a)

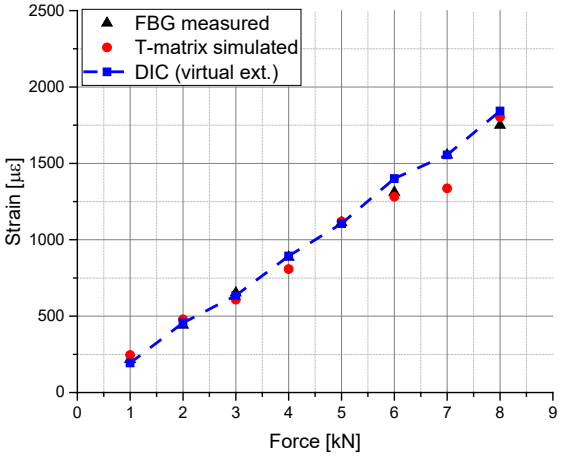

(b)

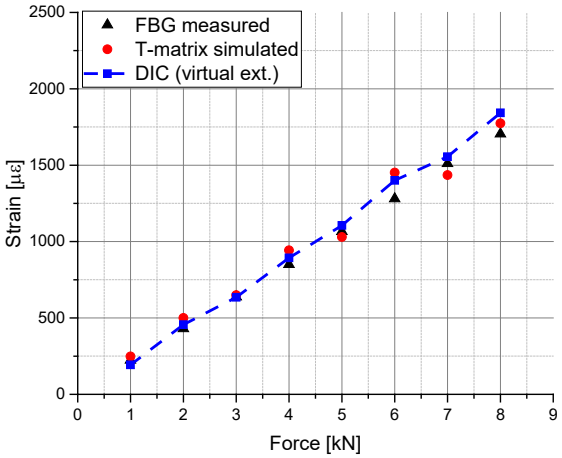

(c)

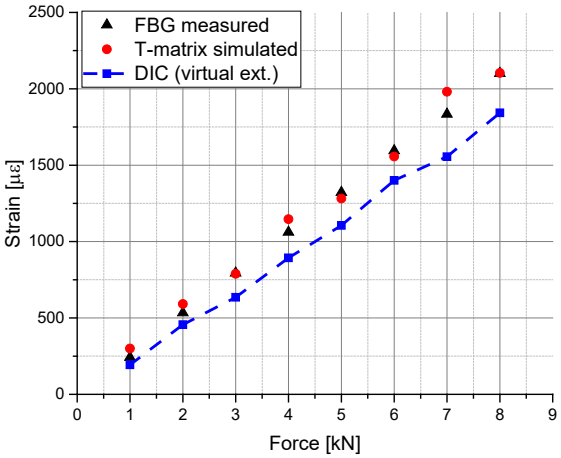

(d)

Fig. 12: Comparison between experimental, simulated and averaged DIC measured strain for an array of four 1mm FBGs: (a) first, (b) second, (c) third and (d) forth FBG grating staring from the left side of the schematized repeating unit structure.

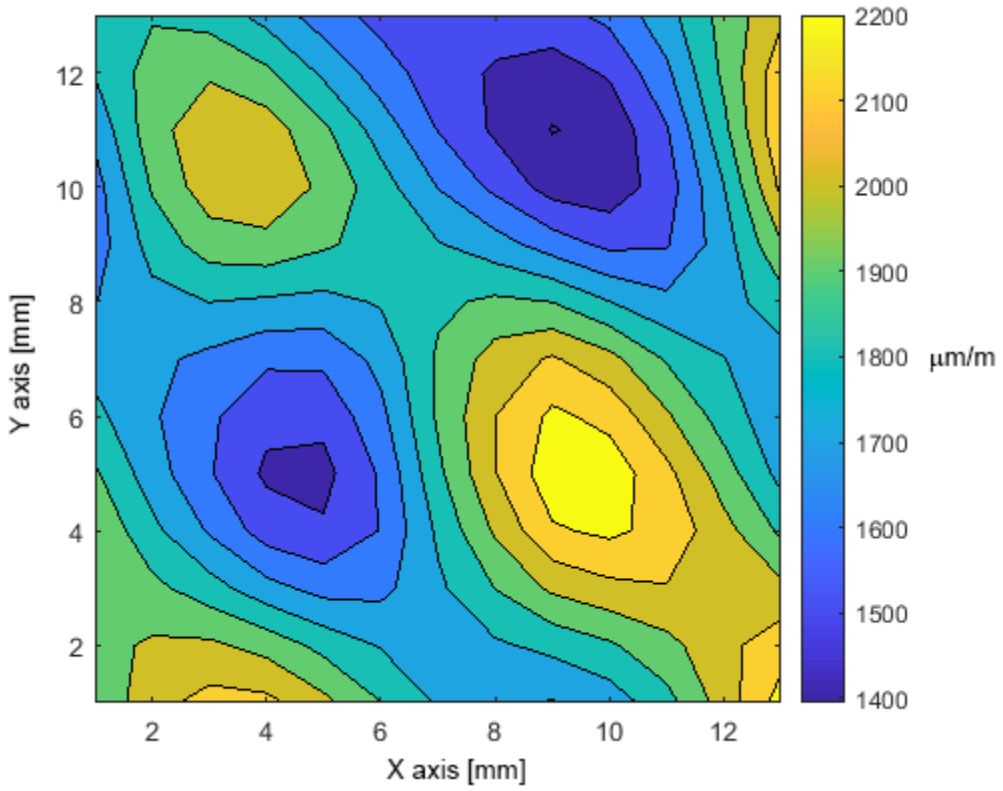

Figure 13: T-matrix simulated response of FBGs of 1 mm length over a 13 mm x 13 mm area of the DIC strain field

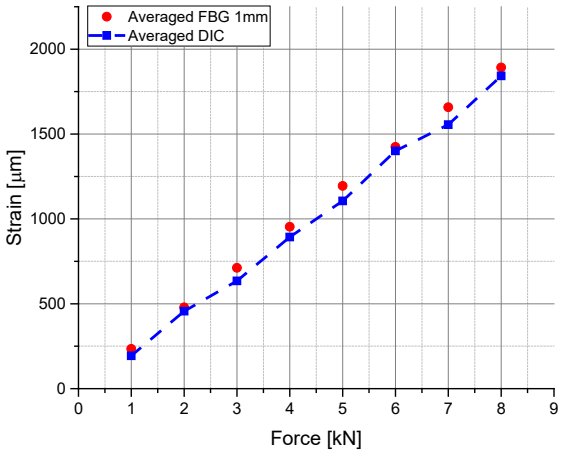

Fig. 14: Comparison between nominal strains and averaged ones regarding FBG 1mm and DIC measurements.

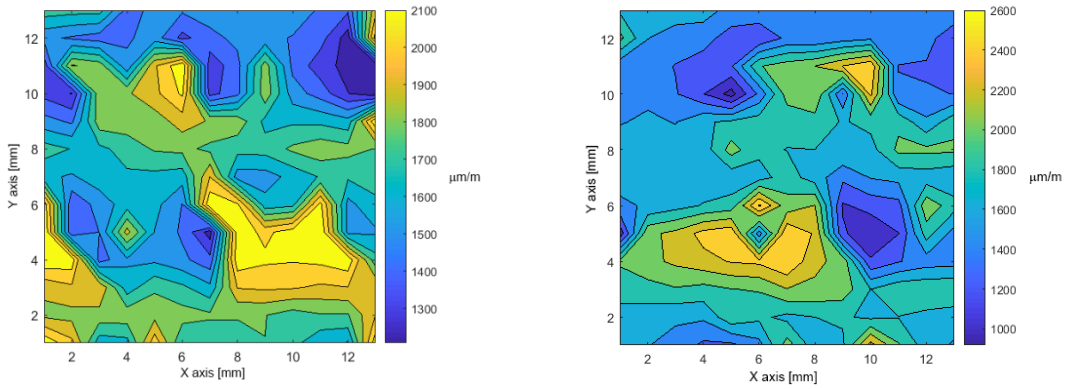

(a) (b)

Figure 15: T-matrix simulated response of FBGs of 6 mm (a) and 12 mm (b) length over a 13 mm x 13 mm area of the DIC strain field